Aerospace Science and Technology 166 (2025) 110571

Contents lists available at ScienceDirect

Aerospace Science and Technology

journal homepage: www.elsevier.com/locate/aescte

Enhancing low-frequency transmission loss in aircraft fuselage sidewalls with a flat array of covered Helmholtz resonators metamaterial

K. Carillo *, L. Pires, T. Padois, V. Brailovski, O. Doutres

Department of Mechanical Engineering, École de technologie supérieure, Montreal, H3C 1K3, Canada

ARTICLE INFO

Edited By: Sirish Namilae

Keywords:
Acoustic metamaterial
Vibroacoustic resonators
Aircraft sound insulation
Finite element modeling

ABSTRACT

This paper explores the use of a flat array of covered Helmholtz resonators (CHRs) as a metamaterial for enhancing the acoustic transmission loss (TL) of aircraft fuselage sidewall. The benefits of CHRs are twofold: (i) decreasing the Helmholtz resonance frequency, thereby targeting lower frequencies, and (ii) providing precise control over the resonant frequency of the metamaterial when integrated into a fuselage sidewall. In this paper, we first examine the vibroacoustic behavior of a single CHR, observing a significant decrease in resonant frequency as the covering plate approaches the neck entrance. Subsequently, we evaluate arrays of CHRs, with different filling factors, and their impact on the TL of an aircraft fuselage sidewall. Placing the CHRs metamaterial in the dead space between stringers improves the TL by up to 10 dB at the panel's ring frequency, demonstrating their potential for low-frequency noise reduction in aircraft.

1. Introduction

Reducing noise inside aircraft is a paramount concern in modern aviation, driven by the need to limit passengers' and crew's exposure to high noise levels, which can cause discomfort and long-term hearing damage. Aircraft noise originates from engines, aerodynamic interactions, and mechanical systems. Conventional acoustic insulation treatments used in aeronautics generally consist of one or more layers of porous materials, placed between the aluminum skin panel and the trim panel of the fuselage sidewall. Although effective at mid and high frequencies, these treatments are limited at low frequencies due to the ability of long wavelengths to penetrate them.

To overcome this issue, numerous subwavelength vibroacoustic metamaterials have been proposed in the literature as they can be finely tuned to target specific low-frequency ranges while having small thickness-to-wavelength ratio [1]. Those metamaterials include locally resonant sonic materials [2,3], membrane-type/plate-type metamaterials [4–6] or structured resonators [7,8]. In particular, different strategies have been explored to integrate Helmholtz resonators (HRs) into double wall structure to enhance system insulation at their resonant frequency. For examples, Narang [9] used studs supporting the walls to create small resonant slits, Mason & Fahy [10] incorporated a frame containing HRs into a double wall structure, and May et al. [11], Prydz et al. [12] and Kuntz et al. [13] used one of the walls to form or attach an array of HRs. Although these solutions yield significant gains at the HRs' resonant frequency, they often compromise the overall performance of the double wall across the frequency range [10,12]. However, installing absorbent material between the walls can mitigate this issue [14].

While effective at low frequencies, HR integration requires space within a double wall. Solutions have been devised to lower HRs' resonant frequency without increasing their size. The presence of porous material within the HR cavity allows for lowering the resonant frequency and broadening the transmission loss (TL) peak but reduces its amplitude [15]. Additionally, the neck shape significantly influences the acoustic response of HRs. Extending the neck into the cavity was proposed [16], and a spiral-shaped neck was explored [17]. Conical or parabolic necks were proposed to enhance the absorption of HRs but slightly increase the resonant frequency [18,19]. Furthermore, the behavior of an HR depends on the surrounding environment, and the proximity of a structure can influence the radiation of the HR's neck. The resonant frequency of an HR installed in a double wall structure can therefore differ from the HR's intrinsic resonant frequency (obtained when the neck radiates into a semi-infinite space). Although it is not explicitly analyzed in this way in ref [13], the results suggest that the resonant frequency of the HR array shifts towards lower frequencies, and the associated TL peak slightly decreases when the HR necks are close to the sound package in the fuselage sidewall. The effect of the environment at the HR necks' openings can also significantly reduce the

* Corresponding author.
E-mail address: kevin.carillo@irsst.qc.ca (K. Carillo).

https://doi.org/10.1016/j.ast.2025.110571
Received 16 July 2024; Received in revised form 21 May 2025; Accepted 28 June 2025
Available online 29 June 2025

efficiency of an array of HRs, which relies on the assumption that all resonators should resonate at the same frequency. While detuned resonators can broaden the frequency range over which the TL increases, they also reduce the peak amplitude of the TL gain [10]. In practice, installing HRs close to a surface (whether absorbent or not) within a structure is difficult to control, and the efficiency of the HR array can be significantly reduced as all HRs may resonate at different frequencies. Based on these observations, the concept of covering HRs with a plate placed in front of the HRs neck emerged within our research team as a metamaterial to enhance the TL of aircraft fuselage sidewalls. The benefits of covered HRs, referred to as CHRs, are twofold: (i) decreasing the resonant frequency of the HRs, thereby targeting lower frequencies, and (ii) providing precise control over the resonant frequency of the HRs when integrated into a fuselage sidewall, ensuring the optimal efficiency of the proposed metamaterial.

In this paper, we explore the application of CHRs as a metamaterial to increase the TL of aircraft fuselage sidewall by taking advantage of the dead space between the stringers, where flat resonators can be accommodated. First, we study the vibroacoustic behavior of a single circular CHR both numerically through finite element (FE) simulations and experimentally through impedance tube measurements, with a particular focus on the influence of the distance between the covering plate and the HR. Second, we analyze the effect of an array of CHRs, either circular or rectangular, with varying filling factors, on the TL of an aircraft fuselage sidewall in both single (skin panel only) and double wall (skin and trim panels) configurations, under diffuse sound field excitation.

2. Methods

2.1. Geometry of CHRs

Fig. 1(a) illustrates the positioning of the CHRs in the dead space between the stringers of the skin panel of a fuselage sidewall. Two versions of the CHR are considered: (i) a circular version that fits in a 100 mm diameter impedance tube to study the system's vibroacoustic behavior (see Fig. 1(b)), and (ii) a rectangular version with larger dimensions to fill the space available between the stringers of the skin panel (see Fig. 1(c)). Both CHRs are designed with a re-entrant neck to maintain a flat profile. Draft angles of at least 9 degrees were incorporated to facilitate demolding during manufacturing (detailed in Section 2.3), and sharp edges were avoided. The covering plates for both circular and rectangular CHRs are circular, with a diameter of 60 mm and a thickness of 1 mm, centered on the neck and located at a distance Δ_l (see Fig. 1(d)). Both versions share the same neck geometry; the only difference lies in the volume of the circular and rectangular cavities. Without the covering plate, both HRs have a thickness of 17 mm to fit within the dead space (22 mm depth) between the stringers of the skin panel.

2.2. Modeling of the circular CHR

In this work, we developed a numerical model of the circular CHR placed in a virtual impedance tube setup using the FE method in COMSOL Multiphysics® 6.1 (Sweden) to study the vibroacoustic behavior of the system. Fig. 1(e) shows the 3D FE model of the CHR in a 100 mm diameter tube filled with air and having acoustically rigid walls. The "Port" boundary condition was applied to set up an incident plane wave at the entrance of the tube (the source) and to prescribe a nonreflecting condition at the end of the impedance tube (the outlet). Only the plane mode propagates in the waveguide. The normal sound transmission loss (nSTL) was computed by the difference between the incident power level ($L_{W,i}$) at the tube entrance and the transmitted power level ($L_{W,t}$) at the end of the impedance tube such that:

$$nSTL = L_{W,i} - L_{W,t}. \tag{1}$$

Two cases are considered. In the first case, the resonator is treated as a rigid material, and the model is purely acoustic, governed by the

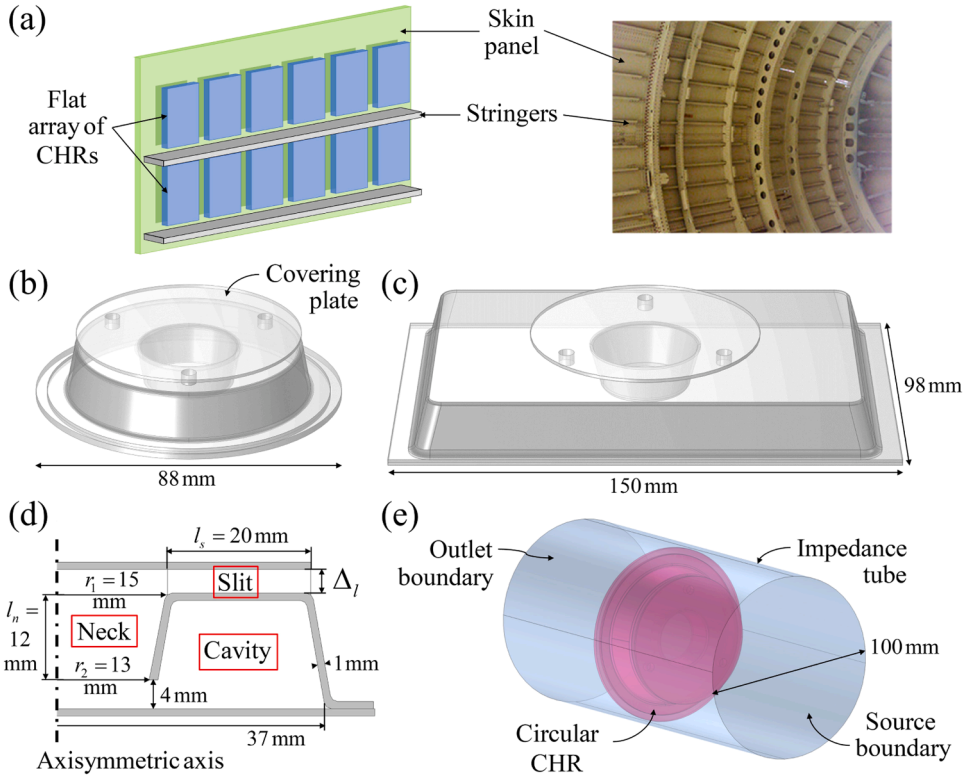

Fig. 1. (a) Schematic of the CHRs positioned between the stringers of the skin panel of an aircraft fuselage sidewall. Geometry of the (b) circular and (c) rectangular CHRs. (d) Cross-sectional view of the circular CHR. (e) FE model of the circular CHR in the impedance tube setup.

Helmholtz equation. The air is modeled as a compressible fluid domain with density $\rho_0 = 1.2$ kg.m^{-3} and sound speed $c_0 = 343$m.s^{-1}. Visco-thermal losses that occur in the neck and in the slit formed between the HR and the covering plate are accounted for using a low reduced frequency model [20]. In the second case, the resonator is modeled as polycarbonate with the following material properties: Young's modulus $E_s = 2.3$ GPa, density $\rho_s = 1200$ kg.m^{-3}, Poisson's ratio $\nu_s = 0.4$, and structural loss factor $\eta_s = 0.01$. Sound propagation in solid domains is governed by the linear elasto-dynamics equation, which relates the linearized displacement field, strain tensor, and stress tensor at all points within the solid domains [21]. At the interface between mechanical and acoustical domains, continuity of stress and normal displacements is assumed. The geometry is meshed using a criterion of at least six 10-noded (quadratic) tetrahedral elements per wavelength at 1.2 kHz (the maximum frequency of interest) to ensure convergence.

2.3. Manufacturing and experimental setups

The circular (Fig. 2(a)) and rectangular (Fig. 2(b)) HRs were both thermoformed from a polycarbonate sheet with a thickness of 1 mm. Polycarbonate material was selected for its lightweight nature, ease of forming, and its existing use in aircraft fuselages to offset insulation blankets from the fuselage skin, thereby reducing moisture buildup [22]. Fig. 2(c) displays the mold used for thermoforming the circular HRs. The circular and rectangular molds were created via 3D printing (fused deposition modeling) using carbon fiber-reinforced nylon with a 100 % infill rate. To minimize thermal deformation during fabrication and ensure repeatability, metal beams were attached to the back of the molds. The covering plates for both circular and rectangular CHRs were cut from polycarbonate sheets using a hole saw. Spacers of 3 mm length were glued between the HRs and the covering plates, setting Δ_l to 3 mm

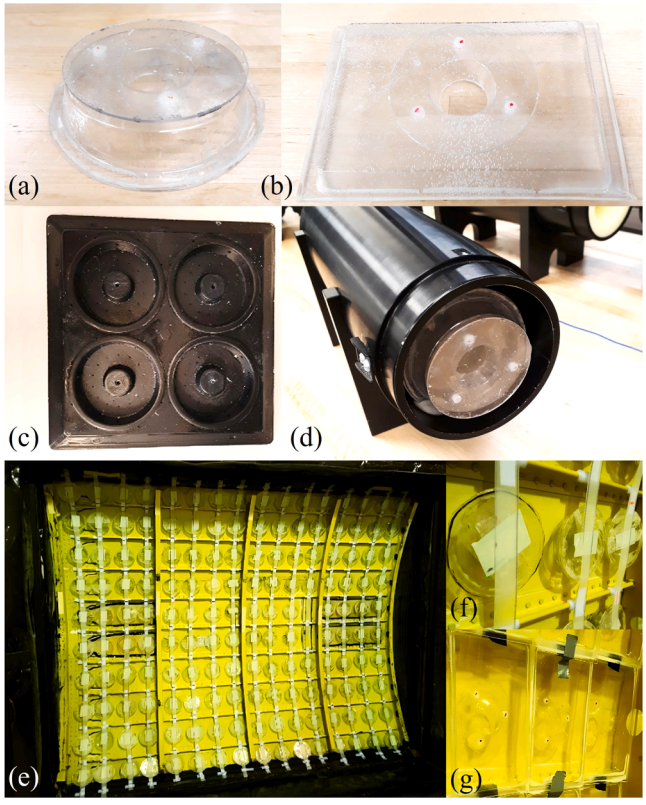

Fig. 2. (a) Circular and (b) rectangular CHRs made of thermoformed polycarbonate. (c) 3D printed mold for the circular CHRs. (d) Impedance tube setup for measuring the nSTL of circular HRs. (e) Large-scale test setup using a fuselage skin panel covered by either (f) circular or (g) rectangular CHRs.

in the experiment. A template was used to center the covering plates onto the HRs. The circular CHRs weighed approximately 22 g, while the rectangular CHRs weighed approximately 47 g.

To assess the nSTL of the circular HRs with and without covering, we used a commercial impedance tube (Mecanum, Canada) as shown in Fig. 2(d), following the ASTM E2611–09 standard [23] and [Ref. 24]. Three samples of circular HRs with and without the covering plate were tested to quantify fabrication variability. Each circular HR was held vertically in the impedance tube using a reusable putty-like adhesive (Blu-tack). Note that the nSTL of rectangular HRs was not assessed using the impedance tube setup as their dimensions significantly exceeded the cross-sectional area of the tube.

Large-scale tests were conducted in coupled reverberant-anechoic rooms of the CRASH (Centre de Recherche Acoustique-Signal-Humain) at the University of Sherbrooke (Fig. 2(e)) following the E-2249–02 standard [25]. A fuselage skin panel measuring 1.7 × 1.45 m^2 with a thickness of 1.3 mm was used. The fuselage, including its stiffening elements, had an equivalent mass per unit area of 8.68 kg/m^2. For the circular CHRs, micro-perforated film was stretched between the stringers (see Fig. 2(f)), and the CHRs were attached to the strips using double-sided adhesive tape. A total of 158 circular CHRs were positioned on the skin panel, resulting in a filling ratio r_n of 30 % and an added mass of 16 % compared to the skin panel alone. For the rectangular CHRs, Velcro was used between the stringers and the surface of the CHRs to allow for a quick and removable attachment. A total of 142 rectangular CHRs were used, increasing r_n to over 70 % with an added mass of 31 % due to their larger size. To mimic an aircraft fuselage sidewall, a porous material mattress (50 mm thick) and a second wall made of composite material with a honeycomb structure were installed above the resonators, forming the double wall configuration. For both single and double wall configurations, careful control of mounting conditions was applied to avoid acoustic leaks. White noise ranging from 100 Hz to 4 kHz was generated by speakers placed in the reverberant room to create the incident diffuse field. The sound transmission loss (STL) was determined from spatially averaged sound pressure level L_p measured in the reverberant room (source side) and spatially averaged sound intensity level L_i measured using an intensity probe in the semi-anechoic room (receiver side) such that [25]:

$$STL = L_p - L_i - 6 - 10\log_{10}(S_m / S), \tag{2}$$

where S is the effective skin panel area (source side), approximately equal to the scanning area S_m (receiver side). To compare the influence of CHRs in single and double wall configurations, the insertion loss (IL) was calculated as the difference between the TL of a given configuration (single or double) with CHRs (circular or rectangular) and the TL of a baseline configuration (single or double) without CHRs, such that:

$$IL = TL_{conf} - TL_{baseline}. \tag{3}$$

3. Results and discussions

3.1. Acoustic behavior of a single CHR

We first analyze the influence of the covering plate on the vibroacoustic behavior of a single CHR. Fig. 3(a) displays the nSTL of the circular CHR as a function of frequency for different distance Δ_l between the HR and its covering plate, computed using the purely acoustical FE model. This system behaves as a single degree of freedom (DOF) resonant system, with maximum nSTL observed at the resonant frequency. The resonant frequency decreases from 1005 Hz when the covering plate is far from the neck entrance and does not influence its acoustic behavior, to 500 Hz when the covering plate is 1 mm from the HR. This significant decrease in resonant frequency, depending on the distance between the covering plate and the HR, demonstrates the benefit of such a system for targeting low frequencies in a minimal volume. It also

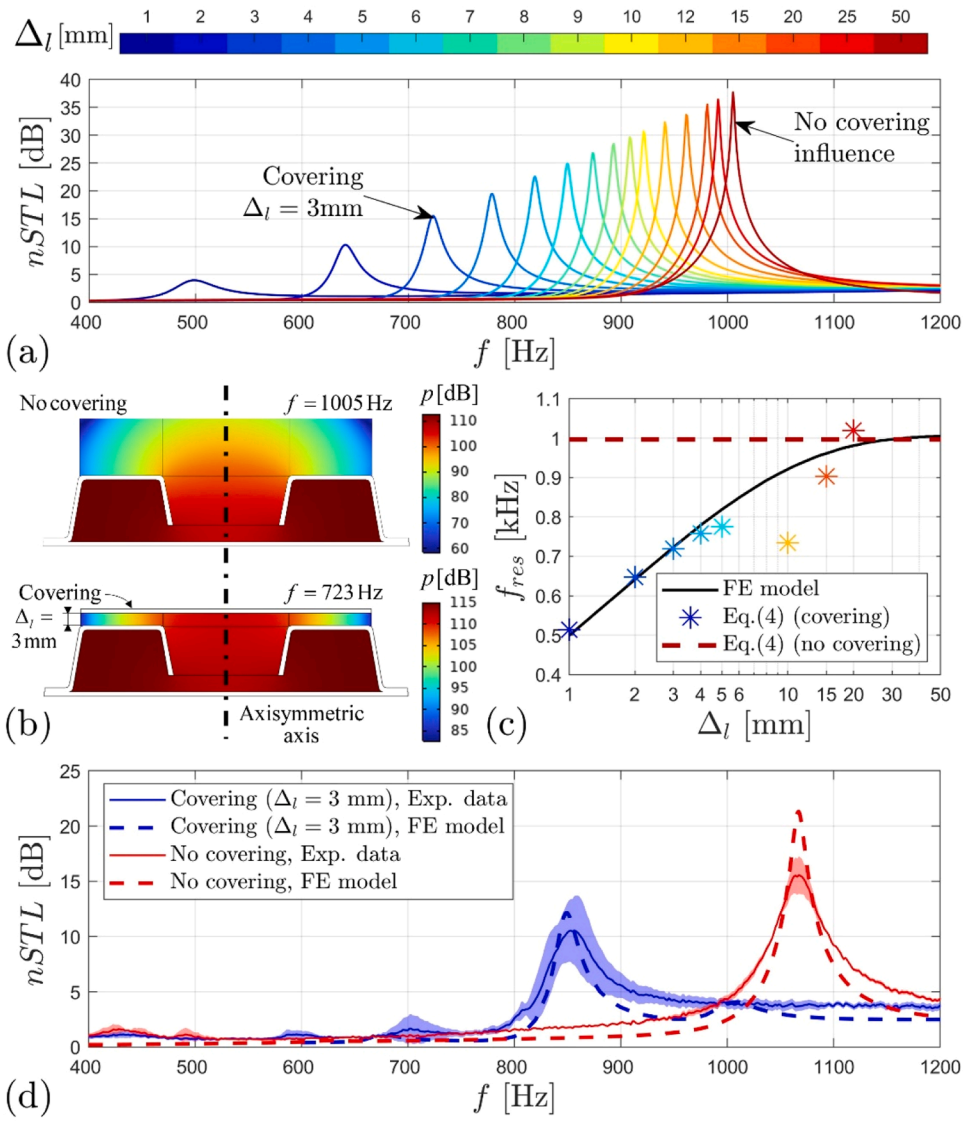

Fig. 3. (a) nSTL of the acoustically rigid circular CHR as a function of frequency for different distance Δ_l from the covering plate (FE model). (b) Acoustic pressure field of the circular HR with and without covering plate (FE model). (c) Resonant frequency of the circular CHR as a function of the distance Δ_l (FE model and Eq. (4) of the analytical model). (d) nSTL of the polycarbonate circular HR with and without covering (experimental data versus FE model).

highlights the necessity of precise control over the distance Δ_l, as the resonant frequency is significantly impacted by this distance.

To further understand the acoustic behavior of the system, Fig. 3(b) displays the sound pressure field inside the CHR in two scenarios: (A) when the covering plate is far from the HR, effectively absent, and (B) when the covering plate is close to the neck of the HR. In the absence of the covering plate, the system behaves as expected: the acoustic pressure varies linearly in the neck, corresponding to the acoustic mass, and is almost homogeneous in the cavity, which acts as the acoustic compliance. When the covering plate is close to the neck of the HR, the radial slit formed between the plate and the HR acts as the acoustic mass, while the former neck together with the cavity act as the acoustic compliance of the system. The maximum nSTL observed in Fig. 3(a) at the resonant frequency of the HRs (whether covered or not) is explained by the fact that, at resonance, the HR placed in the impedance tube imposes a pressure node at the entrance of the neck (i.e., minimum acoustic pressure, as shown in the pressure fields in Fig. 3(b)), leading to minimum acoustic impedance. Consequently, a large part of the acoustic energy is reflected back toward the source, resulting in maximum nSTL. This phenomenon, purely reactive in nature, is typical of the behavior observed in reactive mufflers (see Ref. [26], Section K).

Using the insights from the sound pressure field, it becomes straightforward to approximately predict the resonant frequency of the system in the two previous scenarios (A) and (B) using the classical equation for a 1 DOF mass-spring system:

$$f_{res} = \frac{1}{2\pi\sqrt{M_a C_a}}, \tag{4}$$

where M_a is the acoustic mass of the system and C_a is the acoustic compliance of the cavity. M_a incorporates the acoustic mass of the effective neck M_n and the acoustic mass of radiation $M_{r,1}$ at the entrance and $M_{r,2}$ at the back of the neck, such that $M_a = M_n + M_{r,1} + M_{r,2}$. In scenario (A), when the covering plate is far from the HR, the acoustic mass of the neck is given by $M_n = \frac{\rho_0 l_n}{\pi r_1 r_2}$, while the acoustic masses of radiation are approximated by $M_{r,i} = \frac{8\rho_0}{3\pi^2 r_i}$, where $i \in \{1;2\}$, which is an approximation from circular baffled piston. In scenario (B), when the covering plate is close to the HR, the acoustic mass of the slit is given by $M_n = \frac{\rho_0}{2\pi\Delta_l}\log\left(\frac{r_2+l_s}{r_2}\right)$ while the acoustic masses of radiation $M_{r,i}$ are approximated using length corrections for a baffled rectangular orifice

(see Ref. [26], Section F). In both scenarios, the acoustic compliance of the system is given by $C_a = \frac{V}{\rho_0 c_0^2}$. However, the effective cavity volume V is equal to 5.2×10^4 mm^3 in scenario (A) and 6.2×10^4 mm^3 in scenario (B).

Fig. 3(c) displays the resonant frequency of the system as a function of the distance between the HR and the covering plate. It shows that Eq. (4) provides accurate approximations of the resonant frequency of the system computed using the FE model when the covering plate is either (A) very far from or (B) close enough to the HR. At an intermediate distance Δ_l between the HR and its covering plate, analytically computing the resonant frequency becomes more complex, and Eq. (4) is no longer applicable. The effect of the covering plate is purely reactive and can be interpreted as a neck extension, which increases the effective acoustic mass M_a of the system and lowers f_{res} as Δ_l decreases. For instance, when $\Delta_l = 3$ mm, the acoustic mass of the CHR is $M_a = 111$ kg.m^{-4}, compared to $M_a = 66$ kg.m^{-4} without covering, and f_{res} reduces from 1005 Hz to 723 Hz between the uncovered and covered HRs. Nevertheless, decreasing Δ_l also reduces the nSTL peak (see Fig. 3(a)), as the energy advection of the HR is diminished by the decreasing radiating surface due to the covering plate. Additionally, as the covering plate approaches the HR, viscous losses increase, further contributing to the reduction of the nSTL peak. However, these viscous losses do not significantly influence the system's resonant frequency for $\Delta_l > 1$ mm.

Thus far, the resonator has been considered acoustically rigid to isolate the influence of the covering plate on its behavior. For practical application in aircraft fuselage sidewall without adding excessive mass, the resonators were manufactured from polycarbonate. Fig. 3(d) displays the nSTL of the circular polycarbonate HR measured in an impedance tube and simulated using the FE method, both with and without covering. Simulations and measurements are in good agreement. However, compared to the acoustically rigid structure (see Fig. 3 (a)), the resonant frequency of the polycarbonate HRs (with and without covering, respectively referred to "Covering $\Delta_l = 3$ mm" and "No covering influence" in Fig. 3(a)), is shifted to higher frequencies by around 100 Hz (see Fig. 3(d)), indicating a strong vibroacoustic coupling between the vibratory behavior of the polycarbonate structure and the acoustic mode of the HR. Despite this, the reduction in resonant frequency induced by the covering plate is still observed, showing a frequency shift of 200 Hz (see Fig. 3(d)), similar to the acoustically rigid case (see Fig. 3(a)). Additionally, compared to the acoustically rigid structure, the nSTL peaks are lower for the polycarbonate structure due to structural losses that occur when the system deforms.

3.2. *Influence of an array of CHRs on the TL of an aircraft fuselage sidewall*

We now investigate the benefit of using the CHRs to improve the STL of an aircraft fuselage sidewall. For this purpose, Fig. 4(a) and (b) displays the STL in 1/12th octave bands of the single and the double wall configurations, respectively, both including either no CHRs, circular CHRs or rectangular CHRs. Note that the distance Δ_l between the

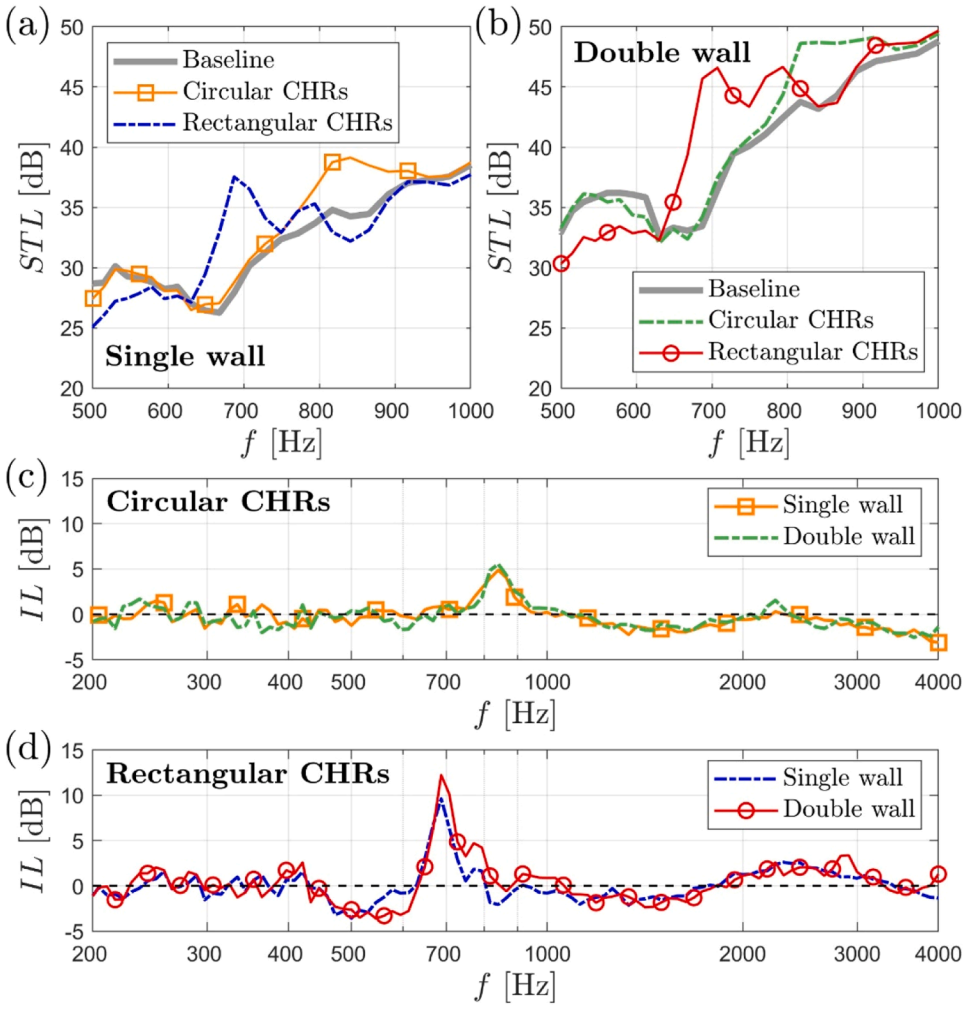

Fig. 4. STL of (a) single and (b) double wall with circular and rectangular CHRs array excited by diffuse sound field, and associated IL for (c) circular and (d) rectangular CHRs. For both circular and rectangular CHRs, the distance Δ_l between the HRs and the covering plates is set to 3 mm.

covering plate and the HRs is fixed at 3 mm for both circular and rectangular CHRs (see Section 2.3), aimed at targeting low frequencies (below 1 kHz) while maintaining significant STL peaks (see Section 3.1). According to Fig. 4(a), the configuration with circular CHRs shows a 5 dB increase in STL around 850 Hz compared to the baseline configuration, which aligns with the resonant frequency of the circular CHRs measured in the impedance tube (see Fig. 3(d)). Hence, the nSTL peak observed for normal incidence excitation of single CHRs in the impedance tube is confirmed under diffuse field excitation of the aircraft sidewall with the circular CHRs. For the configuration with rectangular CHRs, an increase in STL of about 10 dB is observed around 690 Hz compared to the baseline configuration. This frequency is close to the ring frequency of the fuselage skin panel used in this study (see Ref. [8]), which demonstrates the ability of the CHRs array to enhance the STL in this frequency region. In the double wall configuration, similar results are observed regarding the effect of both circular and rectangular CHRs on the STL, as shown in Fig. 4(b).

To facilitate the comparison between the different configurations (single vs. double wall, circular vs. rectangular CHRs), Fig. 4(c) and (d) display the IL, calculated as the difference between the STL of a given configuration including CHRs and the STL of the baseline configuration without CHRs (see Eq. (2) in Section 2.3). It can be observed that the resonant frequency of the rectangular CHRs (around 690 Hz) is significantly lower than that of the circular CHRs (around 850 Hz) due to the larger volume of their cavities. Additionally, the gain in STL for the configuration using rectangular CHRs is notably higher than that for the circular CHRs (10 dB versus 5 dB respectively). However, increasing the filling ratio of CHRs adds weight, which is a critical limitation in aircraft design. Overall, the STL remains almost unchanged across the frequency range (except at the resonances of the CHRs), indicating that CHRs do not significantly affect the acoustic insulation of the aircraft sidewall. The mass added by the CHRs, either circular or rectangular, does not substantially increase the STL of the fuselage panel as the enhancement is sharply localized around their resonant frequencies. Around 500 Hz, however, rectangular CHRs show a 3 dB reduction in the STL performance of the aircraft sidewall. According to additional simulations (not depicted here for the sake of conciseness), this effect originates from an acoustic pressure build-up that occurs between the sidewall and the covering plate. Nevertheless, these results demonstrate the effectiveness of using CHRs in an environment representative of a large-scale aeronautical wall.

4. Conclusion

In this study, we examined the application of a flat array of CHRs as a metamaterial to enhance the TL in double-wall structures, particularly in aircraft fuselage sidewalls. As the covering plate approaches the neck entrance, a significant decrease in the resonant frequency of the system was observed. When the covering plate is close enough, the system effectively transforms into an HR with a radial neck, presenting potential applications as a thin metamaterial for enhancing the acoustic TL of structural walls at low frequencies. As a case study, we implemented an array of these CHRs in the dead space between stringers on an aircraft fuselage sidewall. This implementation led to an improvement in TL of up to 10 dB at the panel's ring frequency. The covering enables precise control over the performance of the HR, independent of the mounting conditions. By controlling the distance between the HR and its covering plate, specific frequencies can be targeted, providing a versatile approach to noise reduction in aerospace applications.

CRediT authorship contribution statement

K. Carillo: Writing – review & editing, Writing – original draft, Software, Methodology, Investigation, Formal analysis, Data curation. **L. Pires:** Writing – review & editing, Methodology, Investigation, Data curation, Conceptualization. **T. Padois:** Writing – review & editing, Supervision, Methodology, Investigation, Conceptualization. **V. Brailovski:** Writing – review & editing, Supervision, Resources, Methodology, Conceptualization. **O. Doutres:** Writing – review & editing, Supervision, Resources, Project administration, Methodology, Investigation, Funding acquisition, Conceptualization.

Declaration of competing interest

The authors declare that they have no known competing financial interests or personal relationships that could have appeared to influence the work reported in this paper.

Acknowledgments

The authors wish to thank the "Ministère de l'économie et de l'innovation – Québec" (MEI), the Consortium for Research and Innovation in Aerospace in Québec (CRIAQ), and the Consortium for aerospace research and innovation in Canada (CARIC) for their financial supports. We also thank Université de Sherbrooke for providing access to the coupled reverberant-anechoic rooms of the CRASH and Patrick Bouché for his assistance during the STL measurements.

Data availability

Data will be made available on request.

References

[1] G. Palma, H. Mao, L. Burghignoli, P. Göransson, U. Iemma, Acoustic metamaterials in aeronautics, Appl. Sci. 8 (2018) 971, https://doi.org/10.3390/app8060971.
[2] Z. Liu, X. Zhang, Y. Mao, Y.Y. Zhu, Z. Yang, C.T. Chan, P. Sheng, Locally resonant sonic materials, Science 289 (2000) 1734–1736, https://doi.org/10.1126/science.289.5485.1734.
[3] K.M. Ho, Z. Yang, X.X. Zhang, P. Sheng, Measurements of sound transmission through panels of locally resonant materials between impedance tubes, Appl. Acoust. 66 (2005) 751–765, https://doi.org/10.1016/j.apacoust.2004.11.005.
[4] Z. Yang, H.M. Dai, N.H. Chan, G.C. Ma, P. Sheng, Acoustic metamaterial panels for sound attenuation in the 50–1000 hz regime, Appl. Phys. Lett. 96 (2010) 041906, https://doi.org/10.1063/1.3299007.
[5] P. Marinova, S. Lippert, O. von Estorff, On the numerical investigation of sound transmission through double-walled structures with membrane-type acoustic metamaterials, J. Acoust. Soc. Am. 142 (2017) 2400–2406, https://doi.org/10.1121/1.5008736.
[6] M. Yao, H. Guo, P. Sun, Y. Wang, X. Xie, C. Xu, Double-panel metamaterial with multi-resonator for broadband sound insulation, Mechanics of Advanced Materials and Structures 32 (8) (2025) 1628–1638.
[7] O. Doutres, N. Atalla, H. Osman, Transfer matrix modeling and experimental validation of cellular porous material with resonant inclusions, J. Acoust. Soc. Am. 137 (2015) 3502–3513, https://doi.org/10.1121/1.4921027.
[8] C. Droz, O. Robin, M. Ichchou, N. Atalla, Improving sound transmission loss at ring frequency of a curved panel using tunable 3D-printed small-scale resonators, J. Acoust. Soc. Am. 145 (2019) EL72–EL78, https://doi.org/10.1121/1.5088036.
[9] P.P. Narang, Transforming wall studs to slit resonator studs for improving sound insulation in walls, Appl. Acoust. 43 (1994) 81–90.
[10] J.M. Mason, F.J. Fahy, The use of acoustically tuned resonators to improve the sound transmission loss of double-panel partitions, J. Sound Vib. 124 (1988) 367–379.
[11] D.N. May, K.J. Plotkin, R.G. Selden, B.H. Sharp, Lightweight sidewalls for aircraft interior noise control, 1985 (No. NAS 1.26: 172490).
[12] R.A. Prydz, L.S. Wirt, H.L. Kuntz, L.D. Pope, Transmission loss of a multilayer panel with internal tuned Helmholtz resonators, J. Acoust. Soc. Am. 87 (1990) 1597–1602.
[13] H.L. Kuntz, R.A. Prydz, F.J. Balena, R.J. Gatineau, Development and testing of cabin sidewall acoustic resonators for the reduction of cabin tone levels in propfan-powered aircraft, Noise Control Eng. J. 37 (1991) 129–142, https://doi.org/10.3397/1.2827801.
[14] S. Sugie, J. Yoshimura, T. Iwase, Effect of inserting a Helmholtz resonator on sound insulation in a double-leaf partition cavity, Acoust. Sci. Technol. 30 (2009) 317–326.
[15] A. Selamet, M.B. Xu, I.-J. Lee, N.T. Huff, Helmholtz resonator lined with absorbing material, J. Acoust. Soc. Am. 117 (2005) 725–733.
[16] A. Selamet, I. Lee, Helmholtz resonator with extended neck, J. Acoust. Soc. Am. 113 (2003) 1975–1985.
[17] C. Cai, C.-M. Mak, X. Shi, An extended neck versus a spiral neck of the Helmholtz resonator, Appl. Acoust. 115 (2017) 74–80.
[18] S.K. Tang, On Helmholtz resonators with tapered necks, J. Sound Vib. 279 (2005) 1085–1096.

[19] E. Gourdon, A.Ture Savadkoohi, B. Cauvin, Effects of shape of the neck of classical acoustical resonators on the sound absorption quality for large amplitudes: experimental results, Build. Acoust. 27 (2020) 169–181, https://doi.org/10.1177/1351010X20910090.
[20] W.R. Kampinga, Viscothermal acoustics using finite elements - Analysis tools for engineers, Ipskamp Printing, 2010 [PhD Thesis - Research UT, graduation UT, University of Twente].
[21] N. Atalla, F. Sgard, Finite Element and Boundary Methods in Structural Acoustics and Vibration, CRC Press, Boca Raton, FL, 2015, pp. 12–13.
[22] R.J. White, D.H. Quimby, B.M. Clark, J.W. Clyne Jr.. U.S. Patent No. 5,398,889, U. S. Patent and Trademark Office, Washington, DC, 1995.
[23] ASTM E2611-09, "Standard test method for measurement of normal incidence sound transmission of acoustical materials based on the transfer matrix method," (American Society for Testing and Materials, New York, 2009), available at https://www.astm.org/e2611-09.html (date last viewed: 20-Jul-23).
[24] Y. Salissou, R. Panneton, O. Doutres, Complement to standard method for measuring normal incidence sound transmission loss with three microphones, J. Acoust. Soc. Am. 131 (2012) EL216–EL222, https://doi.org/10.1121/1.3681016.
[25] ASTM E2249-02 (2016), Standard Test Method for Laboratory Measurement of Airborne Sound Transmission Loss of Building Partitions and Elements Using Sound Intensity (ASTM International, West Conshohocken, PA, 2016).
[26] F.P. Mechel, Formulas of Acoustics, 2nd ed., Springer, Berlin; New York, 2008.